Accepted Manuscript

Novel sound insulation materials based on epoxy/hollow silica nanotubes composites

Xuejun Shi, Jingyi Wu, Xiaoen Wang, Xingping Zhou, Xiaolin Xie, Zhigang Xue

PII: S1359-8368(16)31947-3

DOI: 10.1016/j.compositesb.2017.07.055

Reference: JCOMB 5191

To appear in: *Composites Part B*

Received Date: 13 September 2016

Revised Date: 10 May 2017

Accepted Date: 29 July 2017

Please cite this article as: Shi X, Wu J, Wang X, Zhou X, Xie X, Xue Z, Novel sound insulation materials based on epoxy/hollow silica nanotubes composites, *Composites Part B* (2017), doi: 10.1016/j.compositesb.2017.07.055.

Novel sound insulation materials based on epoxy/hollow silica nanotubes composites

Xuejun Shi, Jingyi Wu, Xiaoen Wang, Xingping Zhou*, Xiaolin Xie, Zhigang Xue*

Key Laboratory for Material Chemistry of Energy Conversion and Storage, Ministry of Education, School of Chemistry and Chemical Engineering, Huazhong University of Science and Technology, Wuhan 430074, China
**Corresponding authors: Tel: +86 27 87793241, Fax: +86 27 87543632*
E-mail addresses: xpzhou@mail.hust.edu.cn; zgxue@mail.hust.edu.cn

Abstract: The performance of a sound insulation material is highly dependent on the technology adopted for its construction. In this study, we synthesized the hollow silica nanotubes (HSNTs) and used them as functional fillers to fabricate a sound insulation nanocomposite based on the epoxy. The sound transmission loss (STL) values of the nanocomposites were measured using a four-microphones standing wave tube. The results showed that for samples with thickness of 3 mm, the STL values of the pure epoxy resin and of nanocomposites with 3 wt% of HSNTs loading were 17 dB and 43 dB, respectively. When the thickness of the nanocomposite increased to 10 mm, the STL value increased to 57.9 dB. The improved sound insulation performances of nanocomposites have been attributed to the unique hollow structure of the hollow silica nanotubes. The mechanical properties and the thermal stability of the nanocomposites were also improved by adding HSNTs into the epoxy matrix.

Keywords: Nanocomposites; Mechanical properties; Interface/interphase; Thermal analysis.

1. Introduction

Noise is a health hazard to which human beings are continuously exposed and therefore, the control of noise pollution has become an important field of research. In general, there are two ways to control noise diffusion [1]. The first way is to actively control the sources of noise. Damping materials can reduce noise in certain machines that produce noise through vibration. This method has been effective to some extent [2-5], however, it is impossible to control all noise sources from machines, which limits the effectiveness of this approach. The second way is a passive method that involves the dampening of the sound wave during its transmission by using sound insulation or sound absorption materials. Sound-absorbing materials are mostly soft and have porous structure, for example, polyurethane foam [6], polypropylene foam [7], foamed rubber [8], open-cell foamed aluminum [9], cotton [10], etc. On the other hand, sound insulation materials are mostly heavy and thick, like steel plates [11] and concrete walls [12]. Fabricating lighter and thinner sound insulation materials would be a great improvement since the utilization of space can be optimized.

In recent years, many people have been working to achieve this objective. Uris and Llopis conducted a study on the sound-proofing property of double-layer composites using rock wool and obtained good results. The sound reduction index for frequencies below 1250 Hz was increased by reducing the rock wool density [13]. Liang studied the sound insulation properties several composites such as polyvinyl chloride (PVC/GB) composite filled with glass beads, a calcium carbonate filled PVC ($PVC/CaCO_3$) composite, and a hollow glass bead-filled polypropylene (PP/HGB)

composite, and found that the sound insulation property of the PP/HGB composite was the best [14]. Ahmadi and Ghasemi measured the sound insulation properties of a nanoclay filled acrylonitrile–butadiene–styrene (ABS) composite and found that ABS/clay (4 wt%) and (8 wt%) improved the sound transmission loss (STL) of a virgin ABS by 6–20 and 4–5 dB at high and low frequency ranges, respectively [15]. Lee and Kang tested the STL and mechanical properties of ABS/carbon-black composites and confirmed that the sound insulation effect was correlated to the amount of carbon black meaning that the higher the content of carbon black, the greater is the sound transmission loss of the composite, and identified the optimum percentage of carbon black for best results [16]. Díaz and Rabanal demonstrated that a multilayer lightweight concrete wall had a better sound-proofing performance for frequencies ranging from 100 to 5000 Hz [17]. A double layer or multilayer insulation material can replace the single layer insulation material to a certain extent, although the double structure has a few drawbacks. For example, if the middle section of the double insulation material is filled with air, an excellent sound insulation effect can be obtained by avoiding the creation of a sound bridge [18, 19]. Therefore, the sound insulation performance of the double layer or multilayer structure of sound insulation material is highly dependent on the construction technology. If the sound bridge is formed or if the bonding layer falls off, the sound insulation effect of the composite material will be greatly reduced.

Yu and Yao developed closed cell aluminum foam sandwich panels (main cell diameter was 3 mm) and proved that this method was effective for sound insulation

[20]. Kim *et al*. investigated the soundproofing properties of polypropylene (PP)/clay /carbon nanotube (CNT) nanocomposites, and found that the STL for the PP/clay (4.8 wt%)/CNT (0.5 wt%) composite was 15-21 dB higher than that for pure PP at high frequencies and 8-14 dB higher at low frequencies [21]. They also measured the PP/CNT/exfoliated graphite nanoplatelet (PP/CNT/xGnP) composites and found that the STL of the PP (80 wt%)/CNT (10 wt%)/xGnP (10 wt%) composite was 5 dB higher than that the pure PP [22].

The results of the above articles have reconfirmed that hollow fillers (CNT, HGB) could improve the sound insulation properties of composite materials. In this study, a typical of hollow silica nanotubes (HSNTs) were synthesized using the sol-gel method refering to the work of the Yadong Yin [23]. It's believed that the hollow silica nanotubes have many applications, such as drug vectors in drug delivery and in controlled drug release [24-26], and acoustic materials. Notably, the interfaces between the silica nanotubes and the epoxy matrix, and the interfaces between silica nanotubes and inner air could scatter, diffract and refract the sound waves energy. Thus, we added HSNTs into epoxy resin (EP) to make the nanocomposites, and anticipated that the materials have a good sound insulation property and therefore will reduce the inherent brittleness of the epoxy [27, 28]. At the same time, it was expected that the nanocomposites will also maintain the excellent performances of the epoxy resin [29-31].

2. Experimental

2.1. Materials

The epoxy resin, diglycidyl ether of bisphenol-A (DGEBA) based E-51 epoxy with an epoxide equivalent weight of 192, was purchased from Shanghai Resin Factory Co., China. Methylhexahydrophthalic anhydride (MeHHPA) hardener was obtained from Jiaxing City Ocean Chemical Co., China. 2-ethyl-4-methylimidazole (EMI-2,4) was used as an accelerant for the curing reaction and was purchased from Beijing Chemical Reagent Co., China.

Polyoxyethylene cetyl ether was purchased from Sigma-Aldrich. Hydrazine hydrate (100%, hydrazine 64%), tetraethyl orthosilicate (TEOS), nickel chloride ($NiCl_2$•$6H_2O$), diethylamine, sodium hydroxide (NaOH), hydrochloric acid (HCl, 37.5%), cyclohexane, ethanol, and isopropanol were supplied from Beijing Chemical Reagent Co., China. All chemicals were used as received without further purification.

2.2. Synthesis of hollow silica nanotubes (HSNTs)

In a typical synthesis procedure [23], 8.0 g of polyoxyethylene cetyl ether was dissolved in 20 mL of cyclohexane at 50^{o}C. 2.0 mL of $NiCl_2$ solution (0.8 M) was added under stirring to obtain a homogeneous solution. Next, 0.50 mL of hydrazine hydrate was added drop wise. After 3 h of stirring, 1 mL of diethylamine and subsequently 3 mL of TEOS were added into the system. The silica coating process was carried out for 4 h during which the TEOS deposited on the surface of the rod-like template to form a coating of silica layer. The coated sample was centrifuged and washed with isopropanol and ethanol. The as-synthesized nickel-hydrazine@silica nanorods were dispersed in 90 mL of HCl solution (3M) to obtain silica nanotubes. The dispersion was stirred at room temperature for 3h. The

silica nanotubes were collected by centrifugation and washed with water and ethanol until the pH value was neutral. The nanotubes were then freeze-dried for 48 h and stored.

2.3. Preparation of EP/HSNTs nanocomposites

The dry HSNTs powder was added directly into the DGEBA epoxy resin using a Rotation-Revolution Hybrid Mixer (ARE-310, THINKY, Japan). The hardener and accelerant were added to the above mixture at room temperature. After mixing for 15 min, the resin mixture was poured into pre-heated steel molds coated with a release-agent and three samples were prepared with different curing temperatures (80 °C for 2 h, 100 °C for 2 h, and 160 °C for 5 h). Then the epoxy (EP)/HSNTs nanocomposites were obtained.

2.4. Characterization

The sound transmission loss (STL) values were measured at room temperature by the standing wave tube as shown in Fig. 1. The test set-up (BSWA Technology Co., Ltd) consist of four 0.25 inch BSWA-MPA416 microphones, a BSWA-CA111 sound calibrator, a type BSWA-SW466 impedance tube, a BSWA-PA50 conditioning amplifier, a BSWA-MC3242 frequency analyzer, and include the BSWA-VA-Lab4 IMP software. Two types of tubes are used: a 30 mm diameter tube (small tube) for high frequencies (1600–6300 Hz) and a 100 mm diameter tube (large tube) for low frequencies (100–2500 Hz). These STL tests method refer to the ASTM E2611 standard.

Transmission electron microscopy (TEM) images were obtained using a Tecnai

G220 electron microscope (FEI Co., Netherlands) with an acceleration voltage of 200 kV. The TEM specimens were cut at room temperature using an ultra-microtome (LEICA Co., Austria, UCT-GA-D/E-1/00) with a diamond knife from an epoxy block in which the films of the nanocomposite were embedded. Thin specimens (50–100 nm) were collected in a trough filled with water and placed on copper grids. Samples were prepared by placing a drop of the HSNT suspension in ethanol on copper grids and dried under ambient conditions. The morphology of HSNTs and their dispersions in the fracture surfaces of the nanocomposites were studied using a field emission-scanning electron microscope (FE-SEM, FEI Co., Netherlands) with an accelerating voltage of 10 kV.

A dynamic mechanical analysis (DMA) was conducted on a TA Instrument (DMA Q800) at a heating rate of 5°C/min and a frequency of 1 Hz. The tests were carried out using the single cantilever mode, the specimen dimensions being 35 × 10.0 × 4.0 mm^3.

Thermogravimetric analysis (TGA) was performed on TA Instruments (TGA Q500) under nitrogen atmosphere over a temperature range of 50–650 °C at a heating rate of 10 °C/min.

Tensile tests and bending tests were carried out using an electronic universal testing machine (Shenzhen San Testing Machine co., CMT4104) with a 10 kN load cell at a crosshead speed of 2 mm/min. Dumbbell-shaped tensile samples were prepared according to the ISO 527 standard and bending tests samples were prepared according to the ISO 14125 standard. The fracture toughness of the samples was

measured according to the ASTM D5045 standard using a three-point-bend (SEN-3PB) single-edge-notch specimen with dimensions 65 × 10 × 4 mm^3. Each reported value was the average from at least six specimens. The charpy impact testing machine (Shenzhen San Testing Machine co., ZBC-1400-1) was used to evaluate the impact resistance of the notch samples. Impacting tests samples were prepared according to the ISO 179 standard. Each reported value was the average of those obtained from at least eight specimens.

2.5. Theoretical basis of STL

In this research, we tested the STL values by changing the boundary conditions of the four sensors measuring method. The samples have to be tested at the absorbent opening end and the absorbent closing end, of the impedance tubes with four microphones. The theoretical STL value was calculated by the equation (1) using a transfer function method [1, 21].

$$STL = -20\lg | t | \quad (1)$$

Where t is the ratio of the transmitting sound energy to the incident sound energy.

The scheme of the measurement is shown in Fig. 1. The sample is in the middle of the tube, the sound wave is produced by the speaker, and four microphones are used to measure the sound power. As shown in Fig. 1 the "**1**" is the incident sound energy, the "**3**" is the transmitted sound energy, and the "**2**" is the reflected sound energy.

3. Results and discussion

According to the mass law of the acoustic, under the same conditions, the materials with higher density will possess higher STL values. In this study, the

densities of the materials were all around 1.20 g/cm^3 with almost no variation, which means that the effect of density on the properties of the nanocomposites can be ignored in the present case [32, 33]. The data of the densities were shown in Table S1 (Supporting Information).

3.1. Dispersion of HSNTs in the epoxy

TEM and SEM were used to examine the morphology of HSNTs and EP/HSNTs nanocomposites. The hollow silica nanotubes (HSNTs) were synthesized by a sol-gel method. From the Fig. 2a, we could see the rod-like template coating by silica. The HSNTs were obtained by washing the template with 90 mL of HCl solution (3M). As shown in Fig. 2b, the HSNTs with a length of 200-450 nm, an inner diameter of 20 nm and an outer diameter of 50 nm were obtained by removing the rod-like template with the HCl. In addition, the N_2 adsorption-desorption isotherms and the pore size distribution of the HSNTs were also tested to prove the hollow structure of the HSNTs (Fig. S1, Supporting Information). From the images of Figs. 2c-f, the nanocomposites with the different HSNTs contents from 0.5 wt% to 3 wt%, it is clear that no epoxy filled the inner cavity of the HSNTs in the composites and the HSNTs kept vacant. It could also be observed that the HSNTs were slightly aggregated throughout the nanocomposites with the 2 wt% and 3 wt% contents.

Fig. 3a show the SEM image of the HSNTs and the Fig .3b show the SEM image of the fracture surface of neat epoxy. Figs. 3c-f, the nanocomposites with the different HSNTs contents from 0.5 wt% to 3 wt%, show that the HSNTs were slightly aggregated when the loading of nanotubes increased and this phenomenon was more

obvious at higher loadings. This is because that the HSNTs have large specific surface areas (81.0 m^2/g) and high surface energies, which causes their aggregation [34-36]. In addition, the strong interaction between the hydroxyl groups on the surface of the HSNTs was also responsible for the aggregation.

3.2. The cross-linking density of the composites

According to the theory of rubber elasticity, the cross-linking density (ρ) of a cured epoxy network is proportional to its storage modulus in the rubbery region [29], and the cross-link density can be calculated using the following equation:

$$\rho = E'/3RT \quad (2)$$

where E′ is the storage modulus at T_g + 30 °C, R is the gas constant, and T is the absolute temperature at T_g + 30 °C. From the DMA results we could get the storage modulus and the absolute temperature.

The curves of the storage modulus (E') and the loss factor versus temperature were given in Fig. 4a and Fig. 4b, respectively. Compared to the neat epoxy, EP/HSNTs nanocomposites showed slightly higher of E' with the HSNTs loading increasing at low temperatures (<100 °C), with the exception of the composites containing 3 wt % HSNTs. However, at higher temperatures (>100 °C), the E' of the neat epoxy is higher than that of the EP/HSNTs nanocomposites. Of course, the storage modulus decreased with the HSNTs loading increasing in this research owing to the phase separation of the epoxy resin and the aggregation of the HSNTs. In Fig. 4b, the curve of the loss factor versus temperature have a lower intensity secondary peak at around 125 °C, in samples with 1.0 wt%, 2.0 wt%, 3.0 wt% HSNTs. This

phenomenon may be due to the phase separation in the epoxy matrix [37-40]. The loss modulus of the nanocomposites shown in Fig. S2 proved the phase separation of the nanocomposites.

Compared with the neat epoxy, the cross-linking densities of the nanocomposites were all decreased with the HSNTs loading increasing. When the content was higher than the 1.0 wt%, the cross-linking densities of the nanocomposites were increased. These results are shown in Fig. 5. Indeed, the cross-linking densities of the EP/HSNTs nanocomposites with 2.0 wt% and 3.0 wt% HSNTs are higher than those of the nanocomposites with 1 wt% HSNTs. This is related to the extent of dispersion of the HSNTs in the epoxy matrix. When the HSNTs content is 1.0 wt%, the dispersion is uniform. However, when the content increased to 2 wt% and 3 wt%, a clear aggregation of the HSNTs was observed owing to an increase in the sizes of the particles. Therefore, the cross-linking density of the nanocomposites with the content of 2 wt%, 3wt% did not reduce significantly.

Based on the above results, we consider that the cross-linking density calculated from equation (2) was an average data, since the HSNTs significantly influence the cross-linking density. When there are no HSNTs, the cross-linking density of the matrix is normal as the neat epoxy and higher than the average data. But in the presence of HSNTs, the cross-linking density of the matrix is decreased and lower than the average data. In this situation, two regions with different cross-linking densities are present in the same epoxy matrix and causes the phase separation [37-40]. This phenomenon may be very useful since the damping properties of the

matrix are improved, which in turn enhances the sound insulation capacity of the nanocomposites.

3.3. Soundproofing properties of the nanocomposites

The STL values were tested from 100 Hz to 6300 Hz and the average STL value was obtained from the 1/3 octave average value [21, 41, 42, 43]. The soundproofing properties and the average STL values of the nanocomposites are shown in Fig. 6 and Fig. 8.

In this typical curves of STL versus sound frequency (Fig. 6a), a lowest STL value appears at the resonance frequency of 1000 Hz for the neat EP, and 1250 Hz for the nanocomposites with 0.5 wt% of HSNTs. Moreover, the curve can be divided into two zones (left zones and right zones) according to sound frequency. When the frequency was lower than the resonance frequency, the STL values of composites decreased with the frequency increasing in left zones. On the contrary, the STL values of composites increased with the frequency increasing in the right zones. In Fig. 6b, the average STL values of the pure epoxy and of the nanocomposites with 3% HSNTs were 45.9 dB and 57.9 dB, respectively. Moreover, the average STL values of the other nanocomposites were also improved. The average STL increase should be due to the unique hollow structure of the HSNTs and this aspect will be explained further through the Fig. 7.

Fig. 7 shows the scheme of the sound wave dispersion into the composites. When the incident sound energy faces the smooth surface of the composite material, part of the sound energy is totally reflected and does not penetrate into the material.

The other part of the sound energy is converted into mechanical vibration and penetrates the composite material, so the sound energy is also decreased. There are several reasons to explain the sound energy dispersion of the composites: firstly**,** it has been that the cross-linking density of the matrix is reduced due to the addition of the HSNTs. The lower cross-linking density of the matrix could improves the damping property, and the damping property of the matrix could absorb the mechanical vibration energy, thus the matrix could dissipate some of the sound energy [3, 44, 45]. Secondly, the pathway through which the mechanical vibration propagated in the composite also plays an important role. The interfaces between the silica nanotubes and the epoxy matrix and the interfaces between silica nanotubes and inner air can scatter, diffract and refract sound waves energy. Thirdly, the air inside the inner cavity of the HSNTs is confined in a narrow space and the air could not move freely which dampened the sound waves in the nanocomposite.

The soundproofing properties and the average STL values of EP/HSNTs nanocomposites with different thickness are shown in Fig. 8. The loading of HSNTs was 3 wt% for all the samples and the thicknesses were from 3mm to 10 mm. The STL value increased with increasing thickness of the samples at all frequencies, and the average STL values of the pure epoxy and the nanocomposites with 3 mm thickness were 17.2 dB and 43.3 dB, respectively. The average STL of the nanocomposites with 10 mm thickness was increased up to 57.9 dB.

This phenomenon may be explained by the fact that the STL value depends on the thickness of the composite. When the material is thicker, the STL value is greater.

Further, when the thickness of the composites is a constant value, a functional filler like HSNT plays an important role in improving the STL value of composites. The sound energy has to pass through the interfaces between the HSNTs and epoxy matrix, and the interfaces between air and HSNTs. Much more interfaces of HSNTs which can scatter, diffract and refract sound waves will greatly extend the propagation path for sound wave. Finally, the sound energy was decreased, resulting from the addition of HSNTs.

It is seen that the nanocomposites significantly improved the sound insulation property. However, these materials also have other interesting properties, such as mechanical properties and thermal stability, hence we have also tested these properties of the nanocomposites.

3.4. Mechanical properties of the nanocomposites

The fracture toughness (K_{IC}) [46], bending, tensile and impact [47, 48] tests were performed to evaluate the mechanical properties of the EP/HSNTs nanocomposites. Fig. 9a shows the fracture toughness of the epoxy resins with different HSNT contents, and the K_{IC} was calculated from equation (3) and (4), where P is the critical load for crack propagation, B is the specimen thickness, W is the specimen width, and a is the initial crack length.

$$K_{IC} = \frac{P}{BW^{1/2}} f\left(\frac{a}{W}\right) \tag{3}$$

$$f\left(\frac{a}{W}\right) = \frac{6x^{1/2}[1.99\text{-}x(1\text{-}x)(2.15\text{-}3.93x+2.7x^2)]}{(1+2x)(1\text{-}x)^{3/2}} \qquad \left(x = \frac{a}{W}\right) \tag{4}$$

The K_{IC} of the pure epoxy resin is 0.62 MPa•$m^{1/2}$ and the K_{IC} of the nanocomposite with 1.0 wt% HSNTs is 0.80 MPa•$m^{1/2}$. The K_{IC} decreased with increasing loading of HSNTs, which may be explained by the increased aggregation of HSNTs at higher loading. However, the K_{IC} of all the EP/HSNTs composites were still higher than that of the pure epoxy.

As shown in Figs. 9b and 9c, the bending strength and tensile strength reached a maximum value when the HSNTs loading was 1.0 wt%. The bending modulus and tensile modulus of the nanocomposites increased only slightly and showed little change when the HSNT loading was increased. This phenomenon may be due to the poor interfacial interaction between the HSNTs and the epoxy matrix.

Fig. 9d shows the Charpy notched impact test results for epoxy resins with different contents of the HSNTs. The impact strength of the pure epoxy resin was 6.25 kJ/m^2 and that of the nanocomposite with 0.5 wt% HSNTs was 11.67 kJ/m^2, yielding an increase of ~86.7%. This obvious toughening effect can be attributed to the lower cross-linking density of the nanocomposites and the plasticizing effect of the nanometer sized particles. Further, the impact strength values monotonously decreased with increase in HSNT loading, which is due to the poor dispersion of the HSNTs into the epoxy matrix at higher loading.

3.5. Thermal stability of the nanocomposites

The Fig. 10 is the TGA curve of the epoxy resin and the nanocomposites with different HSNTs contents. From this fig we could see that, when the loading of HSNTs increases, thermal stability of the nanocomposites was improved, especially at

high temperatures (>400^{o}C). When the temperature was 270^{o}C, the weight loss ratio of all the nanocomposites were less than 1wt%. In general, when the weight loss ratio of the material is 5 wt%, this corresponding temperature is considered to be the initial decomposition temperature of this material [49]. The initial decomposition temperature of the neat epoxy was the 401.3^{o}C, however, the nanocomposites with 1 wt% and 2 wt% HSNTs had a 5 wt% weight loss at 364.4^{o}C and at 400.5^{o}C, respectively, which were lower than that of the neat epoxy. This should be attributed to the decrease of the cross-linking density of the nanocomposites by adding HSNTs. When the content of the HSNTs was up to 3 wt%, the initial decomposition temperature of the composites materials was increased to 417.6 ^{o}C.

This is mainly because that the HSNTs were dispersed into the epoxy matrix and provided large number of hydrogen bonds that act as barriers to prevent the decomposition of the nanocomposites, at the same time, the lower cross-linking density still played a key role and accelerated the decomposition of the nanocomposites [50]. However, this situation gradually changed with increasing loading of HSNTs. Thus, the thermal stability of the nanocomposite was determined by two factors and depended on both the matrix and the filler.

4. Conclusions

The hollow silica nanotubes were synthesized using the sol-gel method and were incorporated without any modification into epoxy resin as functional fillers to prepare EP/HSNTs nanocomposites. Compared with the neat epoxy, the mechanical properties and sound insulation properties of the nanocomposites were all improved. The

cross-linking densities of the epoxy matrix were all decreased with the increased HSNTs loading. In particular, when the thickness of the nanocomposites with 3.0 wt% HSNTs was 10 mm, the average STL value of the sample was increased to 57.9 dB and was higher than the 45.9 dB of the neat epoxy at the same thickness. So we anticipate that adding well dispersed HSNTs to the other polymer matrix will lead to exciting improvements in mechanical properties, thermal stability and so on.

5. Acknowledgement

This work was financially supported by the National Natural Science Foundation of China (51273073, 51622303, and 51210004), National Key Research and Development Program (2016YFB0302402), and Fundamental Research Funds for the Central Universities (2016JCTD112). The authors also gratefully acknowledge the Analytical and Testing Center of HUST for the use of measurement facilities and the Institute of Chemistry, Chinese Academy of Sciences for the sound insulation tests.

6. References

[1] Zhao J, Wang XM, Chang JM, Yao Y, Cui Q. Sound insulation property of wood–waste tire rubber composite. Compos Sci Technol 2010;70(14):2033-8.

[2] Fu Q, Lundin D, Nicolescu CM. Anti-vibration engineering in internal turning using a carbon nanocomposite damping coating produced by PECVD process. J Mater Eng Perform 2013;23(2):506-17.

[3] Gao Y, Wang X, Liu M, Xi X, Zhang X, Jia D. Effect of montmorillonite on carboxylated styrene butadiene rubber/hindered phenol damping material with improved extraction resistance. Mater Design 2014;58:316-23.

[4] Sargianis JJ, Kim H-I, Andres E, Suhr J. Sound and vibration damping characteristics in natural material based sandwich composites. Compos Struct 2013;96:538-44.

[5] Ashworth S, Rongong J, Wilson P, Meredith J. Mechanical and damping properties of resin transfer moulded jute-carbon hybrid composites. Compos Part B: Eng 2016;105:60-6.

[6] Gardner GC, Leary MEO, Hansen S, Sun JQ. Neural networks for prediction of acoustic properties of polyurethane foams. Appl Acoust 2002;64:229-42.

[7] McRae JD, Naguib HE, Atalla N. Mechanical and acoustic performance of compression-molded open-cell polypropylene foams. J Appl Polym Sci 2009:1106-15.

[8] Najib NN, Ariff ZM, Bakar AA, Sipaut CS. Correlation between the acoustic and dynamic mechanical properties of natural rubber foam: Effect of foaming temperature. Mater Design 2011;32(2):505-11.

[9] Han F, Seiffert G, Zhao Y, Gibbs B. Acoustic absorption behaviour of an open-celled aluminium foam. J Phys D: Appl Phys 2003;36(03):294-302.

[10] Binici H, Gemci R, Kucukonder A, Solak HH. Investigating sound insulation, thermal conductivity and radioactivity of chipboards produced with cotton waste, fly ash and barite. Constr Build Mater 2012;30:826-32.

[11] Herrera JM, Recuero M. Influence of seal installation to predict sound insulation of double panel steel doors. Build Environ 2010;45(4):1087-94.

[12] Yoo SY, Jeon JY. Investigation of the effects of different types of interlayers on floor impact sound insulation in box-frame reinforced concrete structures. Build Environ 2014;76:105-12.

[13] Uris A, Llopis A, Llinares J. Effect of the rockwool bulk density on the airborne sound. Appl Acoust 1998;58(1999):327-31.

[14] Liang J-Z. Prediction of sound transmission losses for polymer/inorganic particle composites. Polym Compos 2015;36(11):2059-65.

[15] Ahmadi S, Nassiri P, Ghasemi I, Esmaeilpoor MRM. Sound transmission loss through nanoclay-reinforced polymers. Iran Polym J 2015;24(8):641-9.

[16] Lee JW, Lee JC, Pandey J, Ahn SH, Yeon June K. Mechanical properties and sound insulation effect of ABS/carbon-black Composites. J Compos Mater 2010;44(14):1701-16.

[17] Del Coz Díaz JJ, Álvarez Rabanal FP, García Nieto PJ, Serrano López MA. Sound transmission loss analysis through a multilayer lightweight concrete hollow brick wall by FEM and experimental validation. Build Environ 2010;45(11):2373-86.

[18] Kosny J, Asiz A, Smith I, Shrestha S, Fallahi A. A review of high R-value wood framed and composite wood wall technologies using advanced insulation techniques. Energ Buildings 2014;72:441-56.

[19] Uris A, Bravo JM, Gomez-Lozano V, Guillen I, Llinares J. Experimental sound insulation performance of double frame partitions with slits. Appl Acoust 2008;69(10):918-24.

[20] Yu H, Yao G, Wang X, Liu Y, Li H. Sound insulation property of Al–Si closed-cell aluminum foam sandwich panels. Appl Acoust 2007;68(11-12):1502-10.

[21] Kim M-S, Yan J, Kang K-M, Joo K-H, Pandey JK, Kang Y-J, et al. Soundproofing properties of polypropylene/clay/carbon nanotube nanocomposites. J Appl Polym Sci 2013;130(1):504-9.

[22] Kim M-S, Yan J, Joo K-H, Pandey JK, Kang Y-J, Ahn S-H. Synergistic effects of carbon nanotubes and exfoliated graphite nanoplatelets for electromagnetic interference shielding and soundproofing. J Appl Polym Sci 2013;130(1):3947-51.

[23] Gao C, Lu Z, Yin Y. Gram-scale synthesis of silica nanotubes with controlled aspect ratios by templating of nickel-hydrazine complex nanorods. Langmuir 2011;27:12201-8.

[24] Huang WF, Tsui GCP, Tang CY, Yang M. Fabrication and process investigation of vancomycin loaded silica xerogel/polymer core–shell composite nanoparticles for drug delivery. Compos Part B: Eng 2016;95:272-81.

[25] Gao J, Chen J, Li X, Wang M, Zhang X, Tan F, et al. Azide-functionalized hollow silica nanospheres for removal of antibiotics. J Colloid Interface Sci 2015;444:38-41.

[26] Kumar Rajanna S, Vinjamur M, Mukhopadhyay M. Mechanism for formation of hollow and granular silica aerogel microspheres from rice husk ash for drug delivery. J Non-Cryst Solids 2015;429:226-31.

[27] Kumar K, Ghosh PK, Kumar A. Improving mechanical and thermal properties of TiO_2-epoxy nanocomposite. Compos Part B: Eng 2016; 97:353-60.

[28] Van Velthem P, Ballout W, Horion J, Janssens YA, Destoop V, Pardoen T, et al. Morphology and fracture properties of toughened highly crosslinked epoxy composites: A comparative study between high and low T_g tougheners. Compos Part B: Eng 2016; 101:14-20.

[29] Liu W, Zhou R, Goh HL, Huang S, Lu X. From waste to functional additive: toughening epoxy resin with lignin. ACS Appl Mater Interfaces 2014;6(8):5810-7.

[30] Miao YG, Liu HY, Suo T, Mai YW, Xie FQ, Li YL. Effects of strain rate on mechanical properties of nanosilica/epoxy. Compos Part B: Eng 2016; 96:119-24.

[31] Wang Z, Huang X, Bai L, Du R, Liu Y, Zhang Y, et al. Effect of micro-Al_2O_3 contents on mechanical property of carbon fiber reinforced epoxy matrix composites. Compos Part B: Eng 2016; 91:392-8.

[32] Lee JC, Hong YS, Nan RG, Jang MK, Lee CS, Ahn S-H, et al. Soundproofing effect of nano particle reinforced polymer composites. J Mech Sci Technol 2009;22(8):1468-74.

[33] Wang X, You F, Zhang FS, Li J, Guo S. Experimental and theoretic studies on sound transmission loss of laminated mica-filled poly (vinyl chloride) composites. J Appl Polym Sci 2011;122 (2):1427-33.

[34] Baeza GP, Genix AC, Degrandcourt C, Gummel J, Couty M, Oberdisse J. Mechanism of aggregate formation in simplified industrial silica styrene-butadiene nanocomposites: effect of chain mass and grafting on rheology and structure. Soft Matter 2014;10(35):6686-95.

[35] Rana M, Kumari A, Chauhan GS, Chauhan K. Modified chitosan microspheres in non-aggregated amylase immobilization. Int J Biol Macromol 2014;66:46-51.

[36] Wang Y, Wu X, Yang W, Zhai Y, Xie B, Yang M. Aggregate of nanoparticles: rheological and mechanical properties. Nanoscale Res Lett 2011;6(1):114.

[37] Zhou H-S, Song X-X, Xu S-A. Mechanical and thermal properties of novel rubber-toughened epoxy blend prepared by in situ pre-crosslinking. J Appl Polym Sci 2014;131(22):41110-7.

[38] Fu J-F, Shi L-Y, Yuan S, Zhong Q-D, Zhang D-S, Chen Y, et al. Morphology, toughness mechanism, and thermal properties of hyperbranched epoxy modified

diglycidyl ether of bisphenol A (DGEBA) interpenetrating polymer networks. Polym Advan Technol 2008:1597-1607.

[39] Xu S, Song X, Cai Y. Mechanical properties and morphologies of carboxyl-terminated butadiene acrylonitrile liquid rubber/epoxy blends compatibilized by pre-crosslinking. Materials 2016;9(8):640-652.

[40] Halawani N, Augé JL, Morel H, Gain O, Pruvost S. Electrical, thermal and mechanical properties of poly-etherimide epoxy-diamine blend. Compos Part B: Eng 2017;110:530-41.

[41] Uris A, Maria Bravo J, Llinares J, Estelles H. Influence of plastic electrical outlet boxes on sound insulation of gypsum board walls. Build Environ 2007;42(2):722-9.

[42] Wang X, You F, Zhang FS, Li J, Guo S. Experimental and theoretic studies on sound transmission loss of laminated mica-filled poly(vinyl chloride) composites. J Appl Polym Sci 2011;122(2):1427-33.

[43] Xia L, Wu H, Guo S, Sun X, Liang W. Enhanced sound insulation and mechanical properties of LDPE/mica composites through multilayered distribution and orientation of the mica. Compos Part A: Appl S 2016;81:225-33.

[44] Wu D, Wu L, Wang J, Sun Y, Zhang M. Effect of epoxy resin on the thermal behaviors and viscoelastic properties of poly (phenylene sulfide). Mater Chem Phys 2011;128(1-2):274-82.

[45] Tcherbi Narteh A, Hosur M, Triggs E, Owuor P, Jelaani S. Viscoelastic and thermal properties of full and partially cured DGEBA epoxy resin composites modified with montmorillonite nanoclay exposed to UV radiation. Polym Degrad Stabil 2014;101:81-91.

[46] Wu S, Guo Q, Peng S, Hameed N, Kraska M, Stühn B, et al. Toughening epoxy thermosets with block ionomer complexes: A nanostructure–mechanical property correlation. Macromolecules 2012;45(9):3829-40.

[47] Kumar N, Mireja S, Khandelwal V, Arun B, Manik G. Light-weight high-strength hollow glass microspheres and bamboo fiber based hybrid polypropylene composite: A strength analysis and morphological study. Compos Part B: Eng 2017;109:277-85.

[48] Tian X, Geng Y, Yin D, Zhang B, Zhang Y. Studies on the properties of a

thermosetting epoxy modified with chain-extended ureas containing hydroxyl-terminated polybutadiene. Polym Test 2011;30(1):16-22.

[49] Rafiee F, Otadi M, Goodarzi V, Khonakdar HA, Jafari SH, Mardani E, et al. Thermal and dynamic mechanical properties of PP/EVA nanocomposites containing organo-modified layered double hydroxides. Compos Part B: Eng 2016;103:122-30.

[50] Wang M, Wang C, Song Y, Xie H, Huang Y. One-pot in situ polymerization of graphene oxide nanosheets and poly (p-phenylenebenzobisoxazole) with enhanced mechanical and thermal properties. Compos Sci Technol 2017;14:16-23.

Figure and table captions:

Fig. 1. Scheme of measuring sound transmission loss with a four-microphone impedance tube.

Fig. 2. TEM image: (a) Silica@rod-like template. (b) HSNTs. TEM images of microtome sections (c, d, e, f) of EP/HSNTs composites with different loadings: (c) 0.5 wt%; (d) 1.0 wt%; (e) 2.0 wt%; (f) 3.0 wt%.

Fig. 3. (a) SEM image of HSNTs. (b) SEM image of the fracture surface of pure epoxy and fracture surfaces (b, c, d, e) of EP/HSNTs composites with different loadings: (c) 0.5 wt%; (d) 1.0 wt%; (e) 2.0 wt%; (f) 3.0 wt%.

Fig. 4. The DMA results of the HSNTs nanocomposites.

Fig. 5. The cross-linking densities (ρ) of the neat epoxy and the nanocomposites.

Fig. 6. The soundproofing properties of nanocomposites with different HSNTs contents.

Fig. 7. Scheme of the sound wave dispersion into the nanocomposites.

Fig. 8. The soundproofing properties of nanocomposites with the different thickness.

Fig. 9. (a)Fracture toughness, (b) bending property, (c) tensile property and (d) impact strength of the neat epoxy and the nanocomposites.

Fig. 10. Thermogravimetric results of the neat epoxy and the nanocomposites.

Figure 1

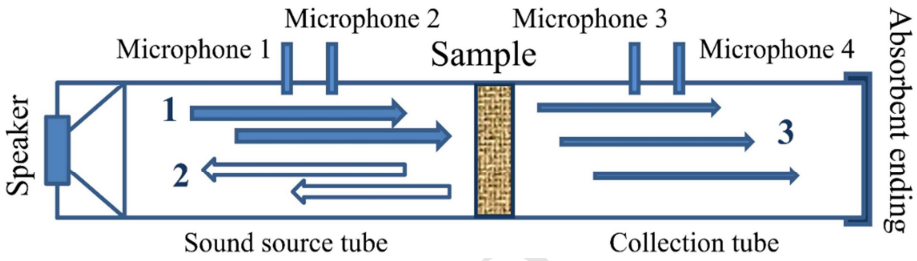

Figure 2

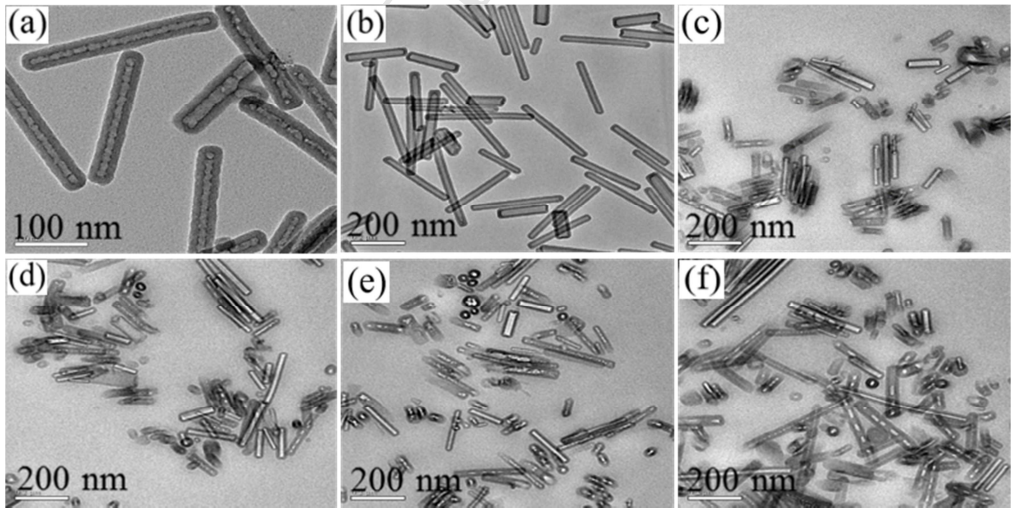

Figure 3

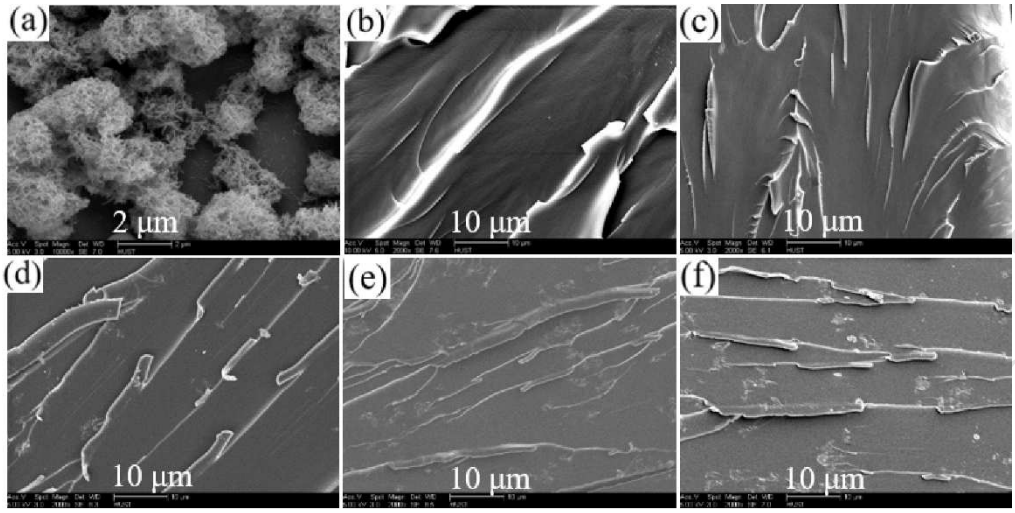

Figure 4

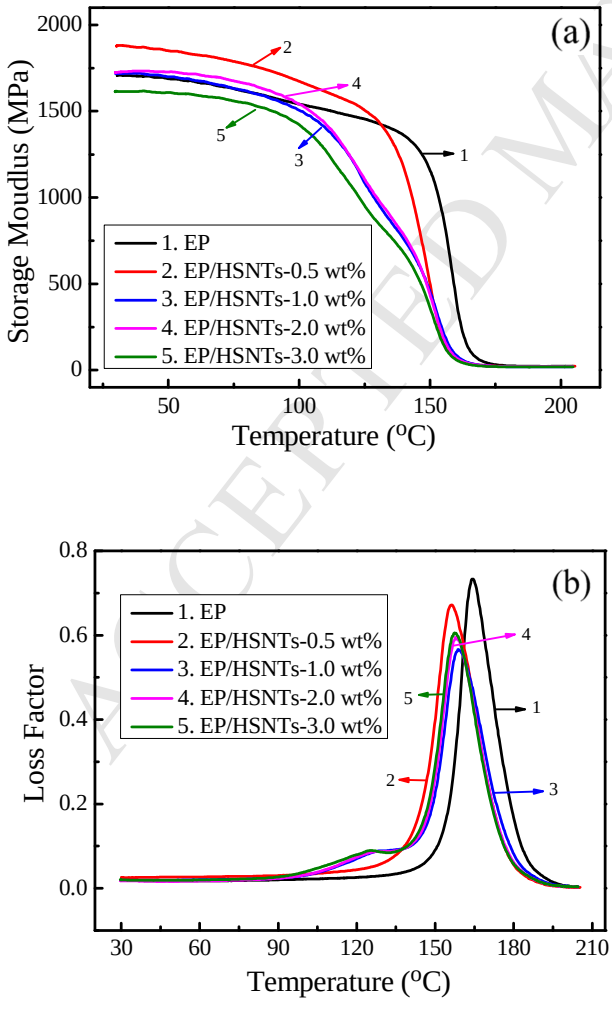

Figure 5

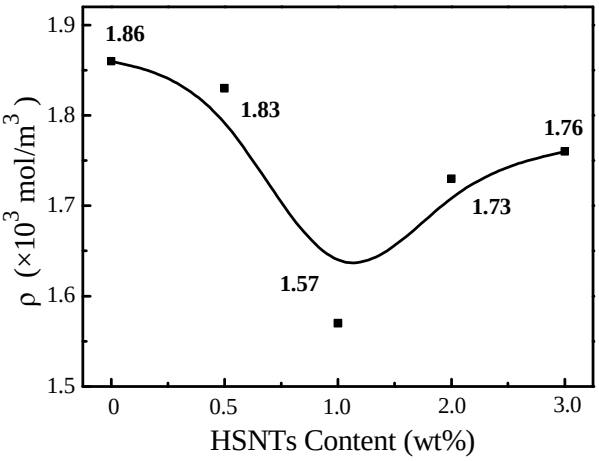

Figure 6

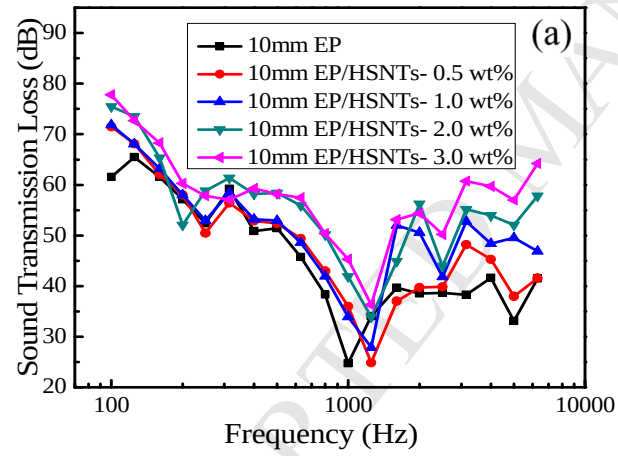

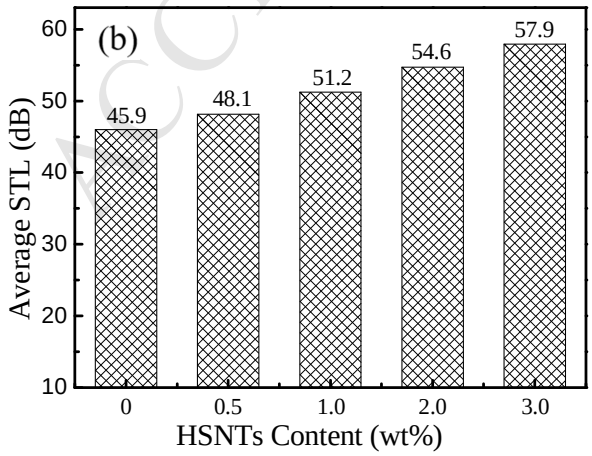

Figure 7

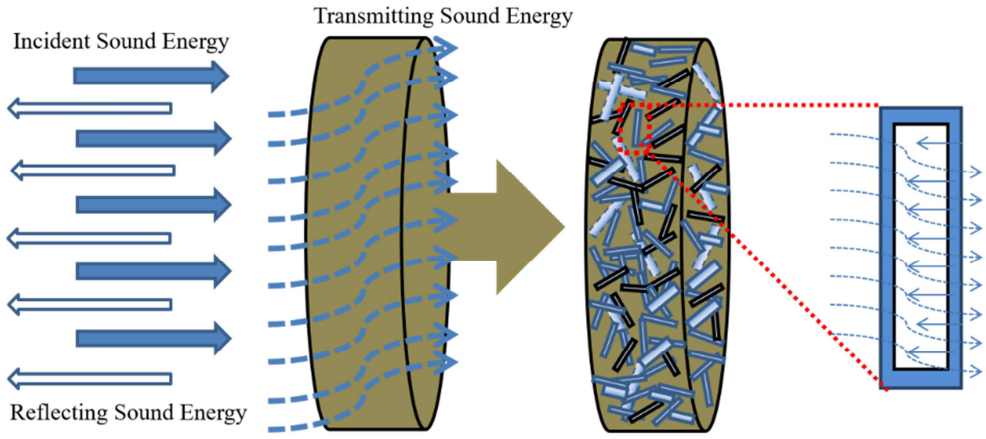

Figure 8

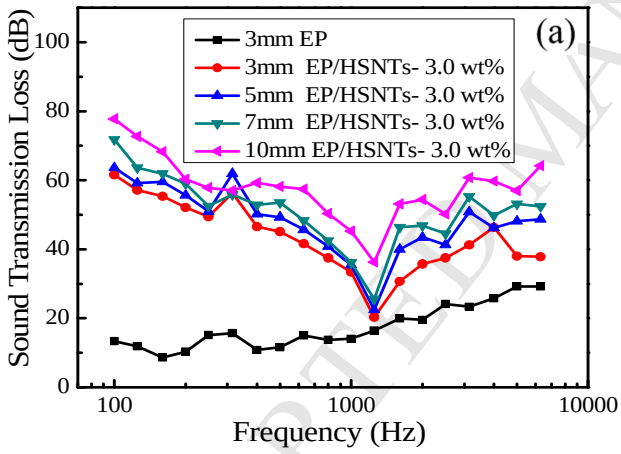

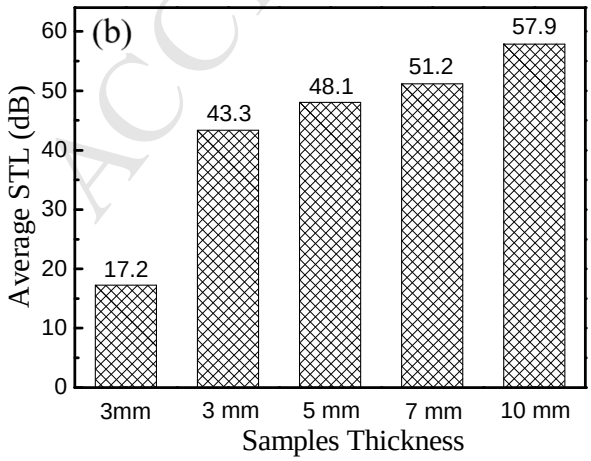

Figure 9

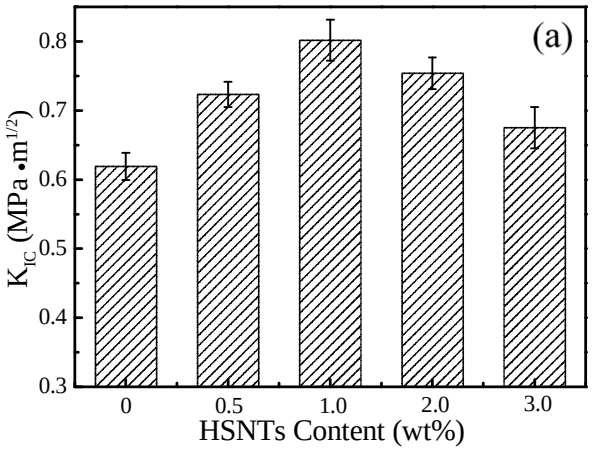
(a)
K_{IC} (MPa •m$^{1/2}$)
0.3
0.4
0.5
0.6
0.7
0.8
0
0.5
1.0
2.0
3.0
HSNTs Content (wt%)

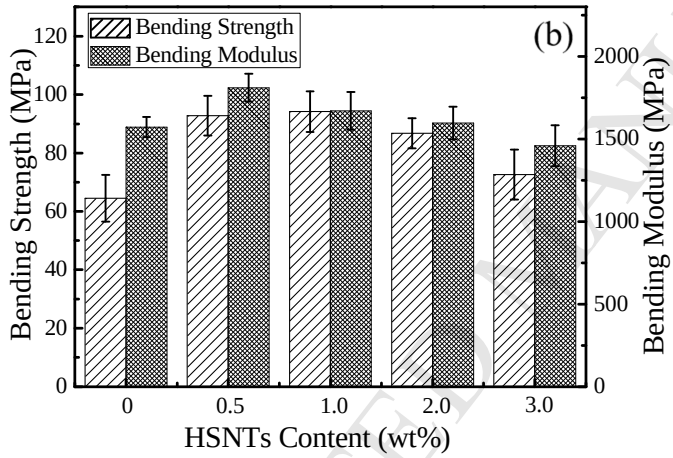
(b)
Bending Strength
Bending Modulus
Bending Strength (MPa)
Bending Modulus (MPa)
0
20
40
60
80
100
120
0
500
1000
1500
2000
0
0.5
1.0
2.0
3.0
HSNTs Content (wt%)

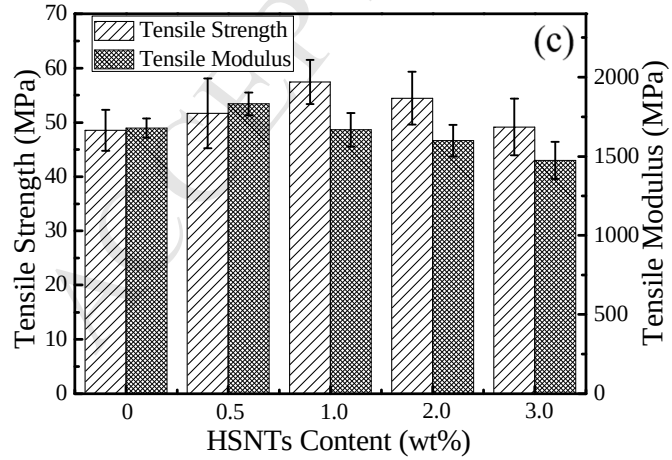
(c)
Tensile Strength
Tensile Modulus
Tensile Strength (MPa)
Tensile Modulus (MPa)
0
10
20
30
40
50
60
70
0
500
1000
1500
2000
0
0.5
1.0
2.0
3.0
HSNTs Content (wt%)

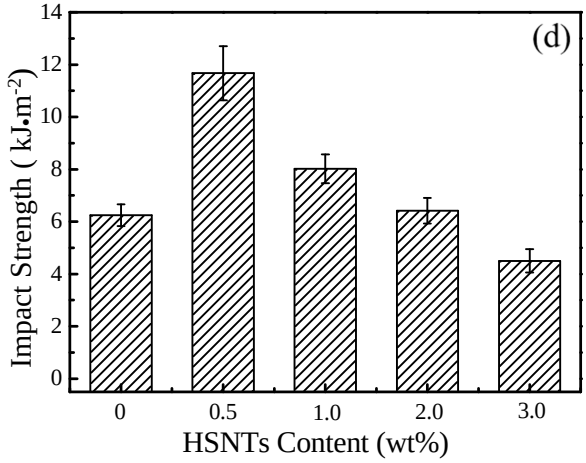

Figure 10